CHEMISTRY OF MATERIALS

pubs.acs.org/cm

Article

First-Principles High-Throughput Screening Pipeline for Nonlinear Optical Materials: Application to Borates

Bingbing Zhang,* Xiaodong Zhang, Jin Yu, Ying Wang, Kui Wu, and Ming-Hsien Lee

Cite This: *Chem. Mater.* 2020, 32, 6772−6779

Read Online

ACCESS | Metrics & More | Article Recommendations | Supporting Information

ABSTRACT: Discovering new nonlinear optical (NLO) materials that require an optimization between multiple properties is a time-consuming and high-cost process. To speed up material development, a first-principles high-throughput screening pipeline for nonlinear optical materials (FHSP-NLO) that combines density functional theory (DFT) codes, linear and nonlinear optical property calculation codes, and data transformation and extraction codes has been developed for searching promising NLO materials from crystals collected in the Inorganic Crystal Scientific Structure Database (ICSD). The tests for a dozen of well-known NLO crystals covering deep-ultraviolet (DUV), UV, vis−NIR, and middle/far-infrared (M-F-IR) wavelength ranges verify the high-accuracy of FHSP-NLO. Subsequently, nearly 300 noncentrosymmetric borates are tested with FHSP-NLO. The screened deep-ultraviolet (DUV) NLO crystals are fully consistent with previously reported results. Besides, five crystals, whose NLO properties have not been reported, i.e., $B_2S_2O_9$, $Al_4B_6O_{15}$, HP-$Na_2B_4O_7$, $KB(SO_3Cl)_4$, and H_3BO_3-3T, are identified as new promising NLO materials. Two hydrated borates $[Ca_2B_5O_9]\cdot[H(OH)_2]$ and $Ca(B_8O_{11}(OH)_4)$, whose second-harmonic generation (SHG) responses are primarily measured, are screened out and suggested to grow large-size crystals for further evaluation. FHSP-NLO provides a powerful and efficient tool to screen and reduce the total number of experiments necessary for searching NLO materials from reported crystals.

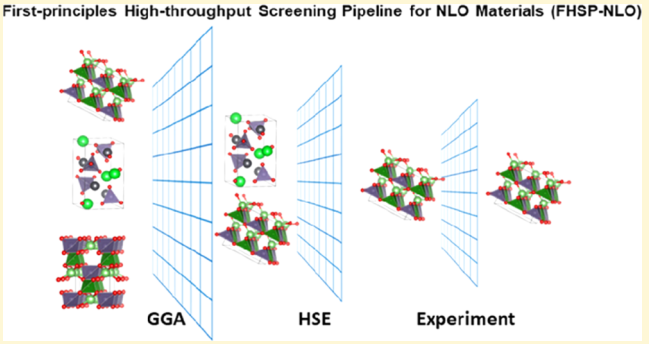

1. INTRODUCTION

Nonlinear optical (NLO) materials are crucial devices achieving frequency conversion for all-solid-state lasers that are widely used in scientific and industrial applications including spectroscopy, free-space communication, generation of entangled photon pairs, and environmental monitoring.[1−4] According to their working wavelength ranges, NLO crystals could be divided into four major categories, i.e., deep-ultraviolet (DUV, <200 nm), ultraviolet (UV, 200−400 nm), visible/near-infrared (vis−NIR, 0.4−3 μm), and middle/far-infrared (M-F-IR, including 3−5 and 8−13 μm atmospheric transparent windows). There are already dozens of commercial NLO materials used in UV and vis−NIR regions, including KH_2PO_4 (KDP),[5] $LiNbO_3$ (LN),[6] $KTiOPO_4$ (KTP),[7] β-BaB_2O_4 (BBO),[8] LiB_3O_5 (LBO),[9] CsB_3O_5 (CBO),[10] and $CsLiB_6O_{10}$ (CLBO).[11] In DUV regions, however, $KBe_2BO_3F_2$ (KBBF)[8] is the only practically usable DUV material to date that can generate coherent light of wavelengths below 200 nm by the direct second-harmonic generation (SHG). But KBBF features strong layered growth behavior, which hinders its applications. In M-F-IR, $AgGaSe_2$, $AgGaS_2$, and $ZnGeP_2$ represent the benchmark IR NLO materials.[12] Nevertheless, low laser damage thresholds (LDTs) intrinsically hinder their practical application. Therefore, the current frontiers of NLO materials research are focused on DUV and M-F-IR regions. Searching for DUV NLO materials that meet the interrelated multiple criteria and M-F-IR NLO materials with high LDTs, large SHG coefficients, and wide IR transparency is urgent and still a challenge.

Discovering and characterizing new materials is a time-consuming and high-cost process. Synthesis of new materials requires a large amount of trial and error to determine optimum synthesis conditions with some chemical reactions taking days to weeks to complete. Once a material is finally synthesized, its properties could be measured. However, NLO materials require an optimization between multiple properties including band gap E_g, birefringence Δn, and SHG coefficients $\chi^{(2)}$. For example, SHG coefficients decrease obviously with an increase in band gap. Besides, birefringence is also inversely proportional to the band gap. Therefore, optimization of NLO materials requires a compromise between these properties and very few materials can reach this balance.

Received: June 19, 2020
Revised: July 15, 2020
Published: July 16, 2020

https://dx.doi.org/10.1021/acs.chemmater.0c02583
Chem. Mater. 2020, 32, 6772−6779

Besides discovering new materials, searching NLO materials from reported crystals with determined structures is another approach. Compared to the tens of thousands of known crystal structures collected in databases such as the Inorganic Crystal Scientific Structure Database (ICSD), only a relatively small number of materials are being actively investigated. Computational assistance can screen and reduce the total number of experiments required rather than experimentally testing every composition. With the development of high-performance computing resources and the improved accuracy of the first-principles methods, predicting and screening new functional materials based on the first-principles approach is receiving increasing attention as a powerful tool to speed up material development. High-throughput screening methods based on density functional theory (DFT) have been successfully applied in the materials science field such as in lithium ion batteries,[13] thermoelectrics,[14] superconductivity,[15,16] and others. However, a high-throughput method that could handle large quantities of materials has not been used in searching NLO materials.

In this work, we developed a first-principles high-throughput screening pipeline for nonlinear optical materials (FHSP-NLO) to search for promising NLO materials from crystals collected in the ICSD. The FHSP-NLO combines the DFT plane-wave codes CASTEP[17] and PWmat,[18,19] optical property analysis codes OptaDOS[20,21] and NewSHG,[22,23] and a data transformation and extraction program. The system could handle large quantities of materials in one go and run automatically. The feasibility and accuracy of FHSP-NLO are tested on a dozen of famous NLO crystals. To test the capability of the system for handling a large number of structures, around 300 noncentrosymmetric (NCS) borate crystals are tested.

2. METHODS

As shown in Figure 1, the only required inputs for FHSP-NLO are crystal structures. The system could handle large quantities of materials from hundreds to thousands or even more in one go and run automatically. The executable number of crystals depends on the computing capacity and time. Generally, chemical composition is one of the useful search keywords to obtain specific materials systems that exhibit similar properties such as band gap and optical transmission region. For example, we can obtain borate crystals by searching structures that include B and O elements. The crystal structures with noncentrosymmetric (NCS) structures could be downloaded as CIF files from the ICSD. Among the downloaded structures, some of them are position-disordered, solid solutions, or with unlocated H atoms. The disordered and incomplete structures will be distinguished and excluded by performing the CIF-check code. Then the CIF files of ordered and determined structures are converted into a .cell format using the cif2cell program as the input file of CASTEP.

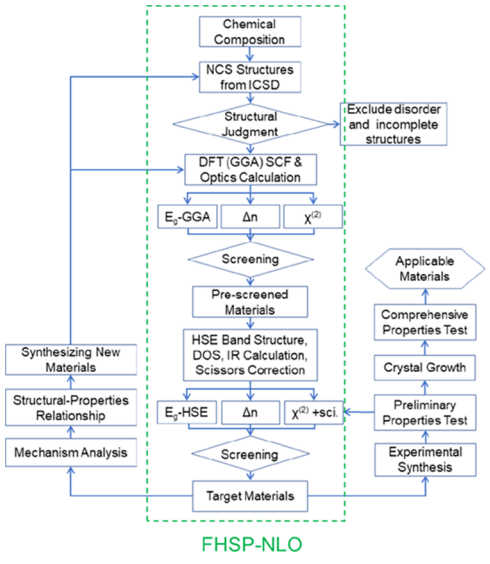

Figure 1. First-principles high-throughput screening pipeline for nonlinear optical materials (FHSP-NLO).

The CASTEP package[17] has been employed to perform self-consistent field (SCF) and optics calculations with the norm-conserving pseudopotentials (NCPs). The exchange−correlation functional was the Perdew−Burke−Ernzerhof (PBE) functional within the generalized gradient approximation (GGA).[24] The plane-wave energy cutoff was set as the maximum value of included atoms at the fine level defined in the pseudopotential file. The SCF calculations were performed with a convergence criterion of 1×10^{-6} eV/atom on the total energy. The Monkhorst−Pack k-point separation for each material is set as 0.07 1/Å in the Brillouin zone for SCF and 0.04 1/Å for optics calculation. The empty bands are set as 3 times the valence bands in the optics calculation to ensure the convergence of refractive index and SHG coefficients. The external pressure is set as 0. The species LCAO states, species pseudopotential files, and species mass are written into a .cell file according to the elements in the crystal.

After completion of the optics calculation, the energy gap E_g, birefringence Δn, and SHG coefficients $\chi^{(2)}$ of crystals could be predicted based on their electronic states. The energy gaps E_g are obtained by calculating the difference between eigenvalues of the lowest unoccupied states and the highest occupied state. The OptaDOS code[20,21] is used to calculate linear optical properties. The imaginary part of the dielectric constant $\varepsilon_2(\omega)$ can be calculated from the electronic transitions between occupied and unoccupied electronic states caused by the interaction with photons.[25] Since the dielectric constant describes a causal response, the real and imaginary parts are linked by a Kramers−Kronig transform. This transform is used to obtain the real part of the dielectric function, $\varepsilon_1(\omega)$. As for crystals with high symmetry including trigonal, tetragonal, hexagonal, and cubic systems, the three optical principal axes are fixed with the crystal axis as well as the Cartesian axis. Thus, the refractive indices along the three principal dielectric axes could be directly calculated depending on the diagonal dielectric constant. As for crystals with low symmetry including triclinic, monoclinic, and orthorhombic systems, the dielectric constants need to be diagonalized and the optical principal axis should be found before calculating the refractive indices. Then the birefringence could be obtained by calculating the difference between the maximum and minimum refractive indices at specific wavelengths. Second-order susceptibility $\chi^{(2)}$ tensors are calculated by the formula proposed by Sipe[26] and developed by Lin and Lee et al. as shown below.[22,23]

$$\chi_{\alpha\beta\gamma}^{(2)} = \chi_{\alpha\beta\gamma}^{(2)}(\mathrm{VE}) + \chi_{\alpha\beta\gamma}^{(2)}(\mathrm{VH}),\ \chi_{\alpha\beta\gamma}^{(2)}(\mathrm{VE})$$
$$= \frac{e^3}{2\hbar^2 m^3} \sum_{vcc'} \int \frac{d^3k}{4\pi^3} P(\alpha\beta\gamma)\, \mathrm{Im}[P_{cv}^{\alpha} P_{cc'}^{\beta} P_{c'v}^{\gamma}] \left(\frac{1}{\omega_{cv}^3 \omega_{vc'}^2} + \frac{2}{\omega_{vc}^4 \omega_{c'v}} \right)$$
$$,\ \chi_{\alpha\beta\gamma}^{(2)}(\mathrm{VH}) = \frac{e^3}{2\hbar^2 m^3} \sum_{vv'c} \int \frac{d^3k}{4\pi^3} P(\alpha\beta\gamma)\, \mathrm{Im}\,[P_{vv'}^{\alpha} P_{cv'}^{\beta} P_{cv}^{\gamma}]$$
$$\left(\frac{1}{\omega_{cv}^3 \omega_{v'c}^2} + \frac{2}{\omega_{vc}^4 \omega_{cv'}} \right)$$

Now, we obtain the energy gap E_g, birefringence Δn, and SHG coefficients $\chi^{(2)}$ of all crystals using GGA functionals. The crystals that meet the criteria of NLO materials applied in a specific wavelength region could be picked out as pre-screened materials. It is generally acknowledged that the band gaps calculated using GGA (E_g-GGA) functionals are always underestimated. Accordingly, the SHG coefficients are overestimated because they are inversely proportional

https://dx.doi.org/10.1021/acs.chemmater.0c02583
Chem. Mater. 2020, 32, 6772−6779

to the band gap. To improve the prediction of the pre-screened crystals, the hybrid functionals based on the screened Coulomb potential Heyd−Scuseria−Ernzerhof (HSE) functional[27,28] are used to get a more accurate band gap (E_g-HSE) by performing the DFT plane-wave code (PWmat) run on GPU machines.[18,19] The scissors operator that is set as the difference between E_g-HSE and E_g-GGA is used to correct their SHG coefficients. Finally, the structures that simultaneously meet the criteria are picked out from the pre-screened structures as target materials.

Subsequently, the samples of target materials could be synthesized to measure the band gap and SHG response. If experimental measurements are consistent with the predicted results, single crystals with large size will be grown for comprehensive testing and application evaluation. On the other hand, the target materials are used to study structure−property relationships using analysis tools such as partial density of states (PDOS), real-space atom cutting, band-resolved $\chi^{(2)}$, and SHG density methods.[29] It will further guide the synthesis of new materials with excellent NLO performance.

3. RESULTS AND DISCUSSION

To test the accuracy of the method, 12 well-known NLO crystals covering DUV, UV, vis−NIR, and M-F-IR wavelength ranges including KBBF,[8] BBO,[8] LBO,[9] CBO,[10] CLBO,[11] KTP,[7] LN,[6] $BaAlBO_3F_2$,[30] SrB_4O_7,[31] $Li_2B_4O_7$,[32−34] BiB_3O_6 (C2),[35] $AgGaS_2$, $AgGaSe_2$, and $ZnGeP_2$[12] are tested. The band gaps using both GGA and HSE functionals E_g-GGA and E_g-HSe, birefringence Δn, and SHG coefficients $\chi^{(2)}$ corrected with the scissors operator of the above NLO crystals are calculated using FHSP-NLO and compared with their measured values using single crystals. The calculated results compared with experimental values are shown in Table 1. We can find that the predicted values show a good agreement with experimental ones. As shown in Figure 2, the squares representing the predicted and experimental values are distributed near the diagonal line that marks the position where the two values are exactly equal. The average absolute error on E_g, Δn, and $\chi^{(2)}$ are 18.3, 29.4, and 27.4%, respectively. The results demonstrate that the methods we used have high accuracy and are reliable in predicting the NLO-related properties.

Borates are preferred systems to search for UV/DUV NLO materials and the vast majority of borates are well studied as NLO materials. Therefore, borate systems are chosen as samples to further test the capability and accuracy of FHSP-NLO. First, we download the CIF files of NCS borates from the ICSD. The searching rule is that B and O are the elements that must be included; the lanthanides, actinides, and transition metals are excluded to ensure a large band gap; and the C element is also excluded to avoid organic−inorganic hybrid crystals. The disordered and incomplete structures are excluded by performing the CIF-check program after downloading it from the ICSD. Finally, 289 crystal structures are successfully calculated by FHSP-NLO. All of the calculations take 3 days on a HP computer cluster with 220 cores. It takes only 5.5 CPU core hours on average for every crystal. The method shows a high efficiency.

The calculated results containing E_g-GGA, refractive indices along the three principal axes, birefringence Δn, nonzero $\chi^{(2)}$ tensors of all of the 289 crystals are listed in Table S1. The Δn and the maximum $\chi^{(2)}$ tensor of borates crystals are plotted against their band gaps E_g-GGA in Figures 3 and 4, respectively. One can easily observe that the trends of Δn and $\chi^{(2)}$ obviously decreased with the increase of their band gap. The statistical results based on the large amounts of

Table 1. Calculated Band Gaps Using GGA and HSE Functionals E_g-GGA and E_g-HSE, Birefringence Δn, and SHG Coefficients $\chi^{(2)}$ Corrected with the Scissors Operator of 12 Well-Known NLO Crystals Compared with Their Experimental Values[a]

crystals	E_g-GGA (eV)	E_g-HSE (eV)	E_g-Expt. (eV)	Δn-Cal.[b]	Δn-Expt.[b]	$\chi_{ij}^{(2)}$(+sci.) (pm/V)	$d_{ij}^{(2)}$ (Expt.) (pm/V)
$AgGaS_2$	0.92	2.16	2.64	0.045	0.053	χ_{36} = 24.08	d_{36} = 11.1 ± 1.7
$AgGaSe_2$	0.53	1.01	1.75	0.054	0.032	χ_{36} = 89.49	d_{36} = 33
$ZnGeP_2$	0.94	2.15	1.67	0.062	0.038	χ_{36} = 116.21	d_{36} = 68.9 ± 10.3
$KTiO(PO_4)$	3.25	5.00	3.54	0.097	0.090	χ_{31} = −7.41, χ_{32} = −5.45, χ_{33} = −6.73	d_{31} = 1.4, d_{32} = 2.65, d_{33} = 10.7
$LiNbO_3$	2.72	4.99	3.1	0.134	0.080	χ_{11} = −20.92, χ_{31} = 14.84, χ_{33} = −53.90	d_{22} = 2.10 ± 0.21, d_{31} = −4.35 ± 0.44, d_{33} = −27.2 ± 2.7
BiB_3O_6-C2	4.75	5.18	4.59	0.149	0.160	χ_{14} = −5.37, χ_{16} = −5.80, χ_{22} = −10.28, χ_{23} = −3.59	d_{14} = 2.4 ± 0.3, d_{16} = 2.8 ± 0.2 d_{22} = 2.53 ± 0.08, d_{23} = 1.3 ± 0.1
$BaAlBO_3F_2$	6.48	6.95	7.52	0.042	0.042	χ_{22} = −χ_{16} = 2.79	d_{22} = 1.24
β-BaB_2O_4	4.79	6.46	6.7	0.128	0.113	χ_{22} = −3.72, χ_{31} = −0.05	d_{22} = 1.60, d_{31} = 0.07
$CsLiB_6O_{10}$	5.18	6.35	6.89	0.063	0.049	χ_{36} = −1.72	d_{36} = 0.74
CsB_3O_5	5.29	7.11082	7.42	0.056	0.063	χ_{14} = −1.69	d_{14} = 1.17 ± 0.11
$KBe_2BO_3F_2$	6.19	7.79	8.43	0.068	0.077	χ_{11} = 1.17	d_{11} = 0.47
LiB_3O_5	6.50	8.28	8	0.06	0.045	χ_{31} = −1.37, χ_{33} = −0.05, χ_{32} = 1.50	d_{31} = −0.83, d_{33} = 0.05, d_{32} = 0.89
$Li_2B_4O_7$	5.76	7.82	7.3	0.055	0.050	χ_{31}−0.18	d_{31} = 0.15
SrB_4O_7	7.35	9.18	8.3	0.004	0.016	χ_{31} = 1.338, χ_{32} = 0.845, χ_{33} = −2.495	d_{31} = 0.8, d_{32} = 1.1, d_{33} = 1.5

[a]Note that $\chi_{ij}^{(2)} = 2d_{ij}^{(2)}$. [b]The calculated and experimental birefringence of $AgGaS_2$, $AgGaSe_2$, and $ZnGeP_2$ are extracted at 5.3 μm, and the values of the other crystals are extracted at 1.064 μm.

https://dx.doi.org/10.1021/acs.chemmater.0c02583
Chem. Mater. 2020, 32, 6772−6779

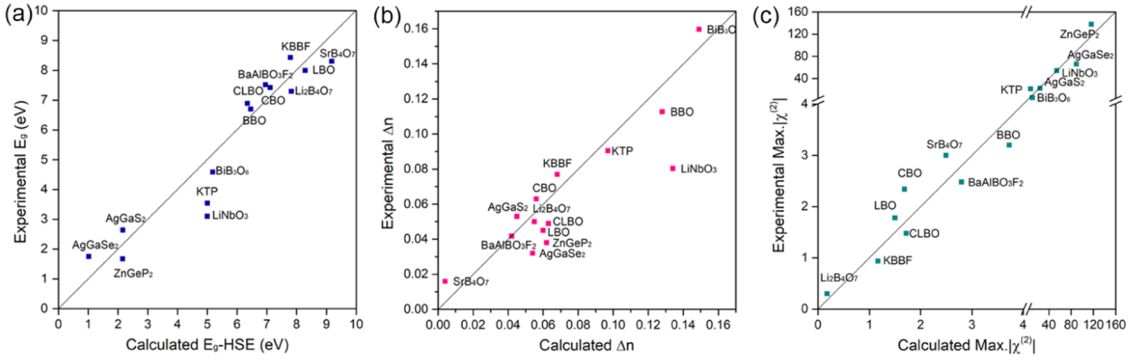

Figure 2. Comparison of calculated and experimental values of well-known NLO materials including (a) E_g-HSE vs measured band gap, (b) birefringence Δn, and (c) maximum SHG coefficients Max. $|\chi^{(2)}|$.

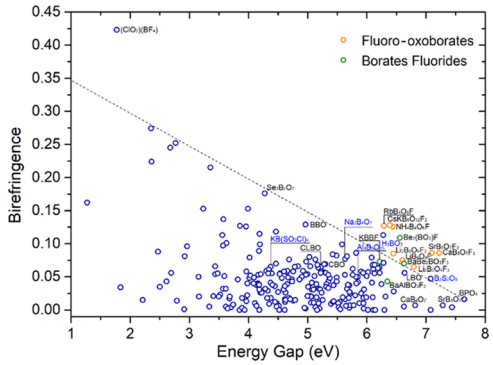

Figure 3. Statistical chart of the calculated band gap vs birefringence at 1064 nm of studied borates.

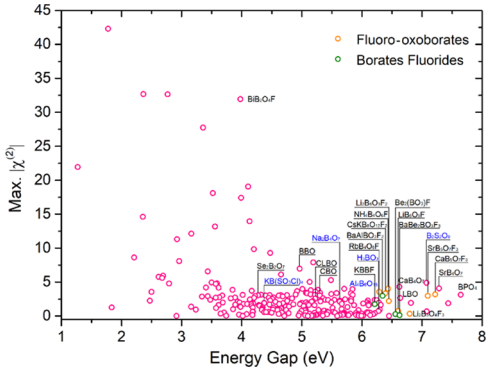

Figure 4. Statistical chart of the calculated band gap vs maximum SHG tensor of studied borates.

borate crystals reveal that the $\chi^{(2)}$ and E_g, as well as the Δn and E_g, are interactive and in inverse proportion with each other, respectively. On the contrary, there is no obvious relationship between Δn and $\chi^{(2)}$ as shown in Figure 5. To evaluate the properties of the borate system as a whole, the statistical average values of linear and nonlinear optical properties of all of the studied borates are calculated. The average E_g, Δn, and maximum $\chi^{(2)}$ are 4.93 eV, 0.05, and 3.24 pm/V, respectively. This reveals that the borate system is suitable and preponderant for searching NLO materials with wide band gaps, appropriate birefringence, and large SHG coefficients.

To screen DUV NLO crystals, the structures that meet the requirements of E_g > 6.0 eV, Δn > 0.06, and $\chi^{(2)}$ > 0.78 pm/V (1 × d_{36} (KDP)) are picked out as listed in Table 2. It is worth noting that all of the selected materials are either

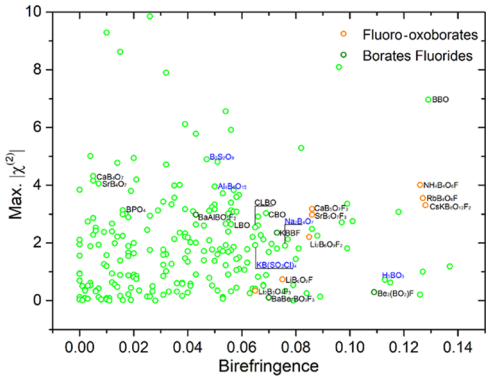

Figure 5. Statistical chart of calculated birefringence at 1064 nm vs maximum SHG tensor of studied borates.

fluorooxoborates or beryllium borate fluorides, including $CaB_5O_7F_3$,[36,37] $SrB_5O_7F_3$,[36,38] $Li_2F_2B_6O_9$,[39] $CsKB_8O_{12}F_2$,[40] $NH_4B_4O_6F$,[41] RbB_4O_6F,[40] $KBe_2BO_3F_2$,[8] $RbBe_2BO_3F_2$,[8] and $NaBe_2BO_3F_2$. As shown in Figure 3, fluorooxoborates and beryllium borate fluorides break the conflicting relationship between the band gap and birefringence of typical borates. In fluorooxoborates, F atoms prevent the appearance of terminal O atoms to avoid the formation of dangling bonds and reducing the band gap. Meanwhile, F atoms break the B−O network and provide an opportunity to construct structures in which BO_3 are coplanarly arranged to generate a large birefringence. As for beryllium borate fluorides, the Be atoms eliminate the dangling bonds of coplanarly arranged BO_3 and keep a balance between the band gap and birefringence. It is worth noting that all of the 10 screened materials have been reported to be able to achieve phase-matching below 200 nm. The results confirmed the accuracy and reliability of FHSP-NLO again.

Although borates have been extensively studied as NLO materials, five crystals, i.e., $B_2S_2O_9$,[42] $Al_4B_6O_{15}$,[43] HP-$Na_2B_4O_7$,[44] $KB(SO_3Cl)_4$,[45,46] and H_3BO_3-3T,[47] are identified as new NLO materials and their NLO properties have not been reported before. Their predicted properties are listed in Table 3.

3.1. $B_2S_2O_9$. $B_2S_2O_9$ consists of vertex-shared BO_4 and SO_4 tetrahedra to form double layers (Figure 6a). It exhibits a colossal band gap of 8.96 eV, a suitable birefringence of 0.047@1064 nm comparable with that of LBO, and a large SHG coefficient χ_{233} = −2.785 pm/V.

3.2. HP-$Na_2B_4O_7$. It was synthesized under high-pressure and high-temperature conditions. As shown in Figure 6b, the

https://dx.doi.org/10.1021/acs.chemmater.0c02583
Chem. Mater. 2020, 32, 6772−6779

Table 2. Calculated Band Gaps E_g-GGA, Birefringence Δn-Cal., and SHG Coefficients $\chi^{(2)}$ of Screened DUV NLO Crystals

ICSD num.	space group	formula	E_g-GGA (eV)	n_1	n_2	n_3	Δn-cal.	$\chi^{(2)}$(pm/V)
264388	$Cmc2_1$	$CaB_5O_7F_3$	7.23	1.591	1.57	1.505	0.086	$\chi_{113} = -3.167$, $\chi_{223} = 1.266$, $\chi_{333} = 2.458$
263469	$Cmc2_1$	$SrB_5O_7F_3$	7.10	1.58	1.561	1.494	0.086	$\chi_{113} = 2.977$, $\chi_{223} = -1.210$, $\chi_{333} = -2.392$
423435	Cc	$Li_2F_2B_6O_9$	6.45	1.58	1.532	1.495	0.085	$\chi_{111} = 0.354$, $\chi_{113} = -1.063$, $\chi_{122} = 2.066$ $\chi_{133} = -2.205$, $\chi_{223} = 1.567$, $\chi_{333} = -0.775$
433805	$P32$	$CsKB_8O_{12}F_2$	6.39	1.614	1.614	1.486	0.128	$\chi_{112} = -3.309$, $\chi_{222} = 3.309$
254161	$Pna2_1$	$NH_4B_4O_6F$	6.44	1.595	1.593	1.469	0.126	$\chi_{113} = -0.053$, $\chi_{223} = 3.519$, $\chi_{333} = -4.012$
433804	$Pna2_1$	RbB_4O_6F	6.29	1.611	1.61	1.484	0.127	$\chi_{113} = 0.125$, $\chi_{223} = -3.480$, $\chi_{333} = 3.549$
77277	$R32$	$KBe_2(BO_3)F_2$	6.16	1.497	1.497	1.43	0.067	$\chi_{112} = 1.870$, $\chi_{222} = -1.870$
260439	$R32$	$Rb(F_2Be_2BO_3)$	6.11	1.526	1.526	1.464	0.062	$\chi_{112} = -1.783$, $\chi_{222} = 1.783$
75594	$C2$	$NaBe_2(BO_3)F_2$	6.28	1.495	1.493	1.424	0.071	$\chi_{112} = -0.298$, $\chi_{123} = 0.791$, $\chi_{222} = 1.970$, $\chi_{233} = -1.676$

Table 3. Predicted Band Gaps E_g-GGA and E_g-HSE, Refractive Index, Birefringence Δn-Cal., and SHG Coefficients $\chi^{(2)}$ of Newly Identified Potential NLO Crystals

ICSD num.	space group	formula	E_g-GGA (eV)	E_g-HSE (eV)	n_1	n_2	n_3	Δn-Cal.	$\chi^{(2)}$ (+sci.) (pm/V)
426544	$C2$	$B_2S_2O_9$	7.08	8.96	1.696	1.671	1.649	0.047	$\chi_{112} = 1.979$, $\chi_{123} = 1.163$ $\chi_{222} = -0.157$, $\chi_{233} = -2.785$
423429	$P3_22$	$Na_2B_4O_7$	5.63	7.25	1.651	1.651	1.574	0.077	$\chi_{112} = -\chi_{222} = -1.128$
10443	Cc	$KB(SO_3Cl)_4$	4.37	6.18	1.652	1.609	1.587	0.065	$\chi_{111} = 0.438$, $\chi_{113} = -0.218$ $\chi_{122} = 0.592$, $\chi_{133} = -0.5284$ $\chi_{223} = 0.150$, $\chi_{333} = 1.138$
54854	$R3$	$Al_4B_6O_{15}$	5.85	7.49	1.696	1.646	1.646	0.050	$\chi_{111} = -\chi_{122} = 0.035$ $\chi_{112} = -\chi_{222} = -0.993$ $\chi_{113} = 1.624$, $\chi_{333} = -2.301$
281322	$P3_2$	$H_3(BO_3)$	6.28	7.77	1.463	1.463	1.350	0.113	$\chi_{111} = -\chi_{122} = 0.033$, $\chi_{112} = -\chi_{222} = 0.008$, $\chi_{113} = \chi_{223} = -0.488$, $\chi_{333} = 0.057$
244721	$C2$	$[Ca_2B_5O_9][H(OH)_2]$	5.82	7.31	1.706	1.663	1.647	0.059	$\chi_{112} = 1.638$, $\chi_{123} = 0.876$ $\chi_{222} = -0.\ 529$, $\chi_{233} = -1.\ 264$
250323	$P2_1$	$CaB_8O_{11}(OH)_4$	5.67	6.75	1.592	1.537	1.511	0.081	$\chi_{112} = 0.216$, $\chi_{123} = 0.397$ $\chi_{222} = 1.291$, $\chi_{233} = -1.248$

https://dx.doi.org/10.1021/acs.chemmater.0c02583
Chem. Mater. 2020, 32, 6772−6779

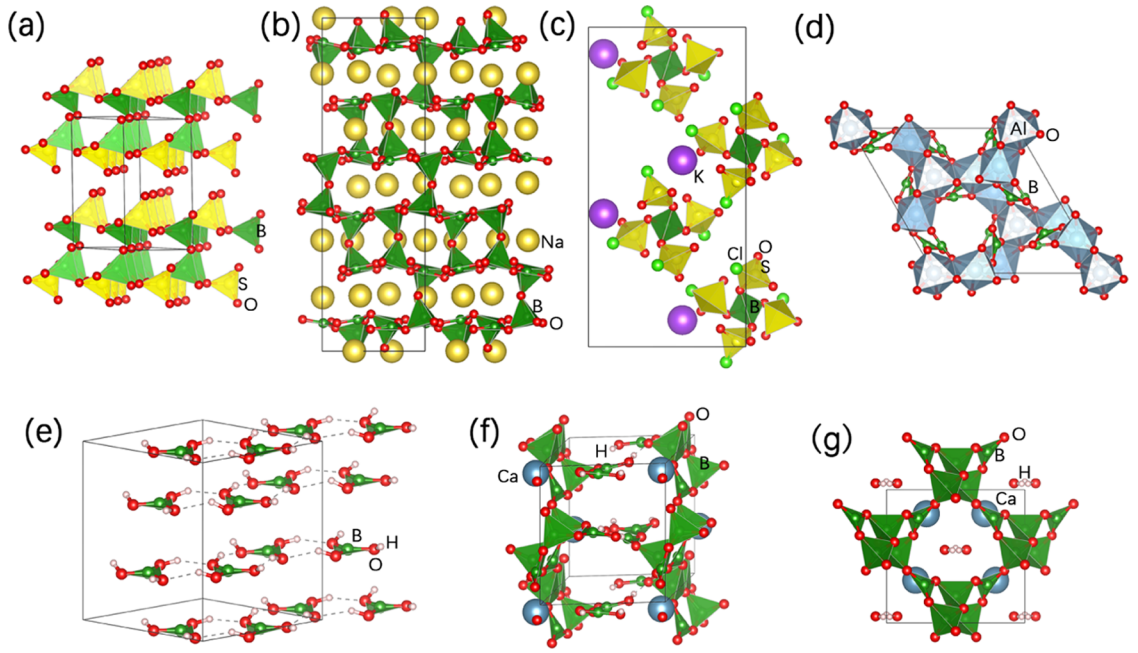

Figure 6. Crystal structures of (a) $B_2S_2O_9$, (b) HP-$Na_2B_4O_7$, (c) $KB(SO_3Cl)_4$, (d) $Al_4B_6O_{15}$, (e) H_3BO_3-3T, (f) $Ca(B_8O_{11}(OH)_4)$, and (g) $[Ca_2B_5O_9]\cdot[H(OH)_2]$.

structure is built from "sechser" rings of alternating vertex-sharing BO_4 and BO_3 groups forming layers in the *ab*-plane. The layers are interconnected to a three-dimensional network structure, forming channels along the *c*-axis in which sodium ions are situated. In HP-$Na_2B_4O_7$, BO_3 groups are coplanarly aligned, which gives rise to a large birefringence. In addition, all O atoms are connected with two B atoms that are beneficial to obtain a large band gap by eliminating dangling bonds on O atoms. To the best of our knowledge, HP-$Na_2B_4O_7$ is the only borate that achieves the compromise between birefringence and band gap for phase-matching in the DUV region that does not contain F, Be, or $(OH)^{-1}$. Therefore, it exhibits a large band gap of 7.25 eV and birefringence of 0.077 with a maximum SHG coefficient tensor χ_{222} = 1.128 pm/V.

3.3. $KB(SO_3Cl)_4$. In potassium tetrachlorosulfatoborate, the isolated anionic structure $B(SO_3Cl)_4$ consists of a B atom tetracoordinated to four SO_3Cl moieties with one O atom (Figure 6c). SO_3Cl are heteroleptic-coordinated anionic groups that can induce polarizability anisotropy and hyperpolarizability. As a result, $KB(SO_3Cl)_4$ shows a large birefringence of 0.065 and a remarkable SHG coefficient tensor χ_{333} of 1.138 pm/V. The band gap is 6.18 eV, which is slightly smaller than those of the other four crystals.

3.4. $Al_4B_6O_{15}$. In $Al_4B_6O_{15}$, Al atoms are connected with six O atoms as octahedroa that shares three edges with the neighboring octahedroa and is further connected with B_2O_5 groups by sharing the vertex (Figure 6d). It achieves a balance between the three properties with band gap, birefringence, and the maximum SHG coefficient being 7.49 eV, 0.05, and χ_{333} = −2.301 pm/V, respectively.

3.5. H_3BO_3-3T. It crystallizes in the $P3_2$ space group, one of the phases of orthoboric acid, and consists of sheets of hygrogen-bonded $B(OH)_3$ molecules connected by van der Waals forces between the sheets (Figure 6e). It shows a wide band gap of 7.77 eV with a large birefringence of 0.113 at 1064 nm. The largest SHG tensor χ_{333} is 0.057 pm/V, which is slightly smaller than that of d_{36} (KDP).

Besides the above five crystals, two hydrated borates, i.e., $[Ca_2B_5O_9]\cdot[H(OH)_2]$[48] and $Ca(B_8O_{11}(OH)_4)$,[49,50] are identified as potential NLO materials (Figure 6f,g). Their NLO effects have previously been measured using powder samples. As shown in Table 3, $[Ca_2B_5O_9]\cdot[H(OH)_2]$ shows a wide band gap of 7.31 eV with a large birefringence of 0.059. The maximum SHG coefficient χ_{112} is 1.638 pm/V. The measured powder SHG response of $[Ca_2B_5O_9]\cdot[H(OH)_2]$ is 3.5 times that of KDP and is phase matchable. The UV cutoff edge of $[Ca_2B_5O_9]\cdot[H(OH)_2]$ is below 190 nm. The predicted results are consistent with the experimental results. $CaB_8O_{11}(OH)_4$ shows a band gap of 6.75 eV and the maximum SHG coefficient is 1.291 pm/V. It exhibits a larger birefringence of 0.081 compared with that of $[Ca_2B_5O_9]\cdot[H(OH)_2]$ as listed in Table 3. Hu et al. grew the crystal with millimeter size and tested the SHG effects and transmission spectrum. It exhibited a SHG response 1−2 times that of KDP and a UV cutoff edge of less than 200 nm. The values are in good agreement with our calculated results. Considering the excellent multiple properties, large-size crystals should be grown for further evaluation.

4. CONCLUSIONS

In summary, we developed a first-principles high-throughput screening pipeline for nonlinear optical materials (FHSP-NLO) that combine DFT codes, linear and nonlinear optical property analysis codes, and data transformation and extraction codes. The system could handle large quantities of materials from hundreds to thousands in one go and run automatically. The feasibility and accuracy of FHSP-NLO are tested on a dozen of well-known NLO crystals covering DUV, UV, vis−NIR, and M-F-IR wavelength ranges. The method shows high accuracy with the average absolute error in E_g, Δn, and $\chi^{(2)}$ being 18.3, 29.4, and 27.4%, respectively. The tests on almost 300 borates further confirm the capability and high efficiency of FHSP-NLO. Besides, five crystals $B_2S_2O_9$, $Al_4B_6O_{15}$, HP-$Na_2B_4O_7$, $KB(SO_3CI)_4$, and H_3BO_3-3T are identified as new

https://dx.doi.org/10.1021/acs.chemmater.0c02583
Chem. Mater. 2020, 32, 6772−6779

promising NLO materials. Two hydrated borates $[Ca_2B_5O_9]\cdot[H(OH)_2]$ and $Ca(B_8O_{11}(OH)_4)$ are suggested to grow large-size crystals. FHSP-NLO provides a powerful and efficient tool for searching NLO from reported crystals collected in the database.

■ ASSOCIATED CONTENT

Supporting Information

The Supporting Information is available free of charge at https://pubs.acs.org/doi/10.1021/acs.chemmater.0c02583.

Chemical formula, ICSD number, space group, predicted band gap, birefringence, SHG tensors $\chi^{(2)}$ (pm/V), crystal structural representations and descriptions of all 289 structures (PDF)

■ AUTHOR INFORMATION

Corresponding Author

Bingbing Zhang − *Key Laboratory of Medicinal Chemistry and Molecular Diagnosis of the Ministry of Education, Key Laboratory of Analytical Science and Technology of Hebei Province, College of Chemistry and Environmental Science, Hebei University, Baoding 071002, China;* orcid.org/0000-0002-1334-5812; Email: zhangbb@hbu.edu.cn

Authors

Xiaodong Zhang − *Key Laboratory of Medicinal Chemistry and Molecular Diagnosis of the Ministry of Education, Key Laboratory of Analytical Science and Technology of Hebei Province, College of Chemistry and Environmental Science, Hebei University, Baoding 071002, China*

Jin Yu − *Key Laboratory of Medicinal Chemistry and Molecular Diagnosis of the Ministry of Education, Key Laboratory of Analytical Science and Technology of Hebei Province, College of Chemistry and Environmental Science, Hebei University, Baoding 071002, China*

Ying Wang − *Key Laboratory of Medicinal Chemistry and Molecular Diagnosis of the Ministry of Education, Key Laboratory of Analytical Science and Technology of Hebei Province, College of Chemistry and Environmental Science, Hebei University, Baoding 071002, China;* orcid.org/0000-0001-6642-543X

Kui Wu − *Key Laboratory of Medicinal Chemistry and Molecular Diagnosis of the Ministry of Education, Key Laboratory of Analytical Science and Technology of Hebei Province, College of Chemistry and Environmental Science, Hebei University, Baoding 071002, China;* orcid.org/0000-0001-8242-4613

Ming-Hsien Lee − *Department of Physics, Tamkang University, New Taipei City 25137, Taiwan*

Complete contact information is available at: https://pubs.acs.org/10.1021/acs.chemmater.0c02583

Funding

The authors declare the following competing financial interest: B.Z. has filed a provisional software copyright application related to this work.

Notes

The authors declare no competing financial interest.

■ ACKNOWLEDGMENTS

This work was supported by the National Natural Science Foundation of China (Grant Nos. 51702356, 21975062, and 51872324), the Natural Science Foundation of Hebei Province (Grant Nos. B2019201433 and E2019201049), and the Western Light Foundation of CAS (Grant No. 2016-QNXZ-B-9).

■ REFERENCES

(1) Tran, T. T.; Yu, H.; Rondinelli, J. M.; Poeppelmeier, K. R.; Halasyamani, P. S. Deep Ultraviolet Nonlinear Optical Materials. *Chem. Mater.* **2016**, *28*, 5238−5258.

(2) Guo, S.-P.; Chi, Y.; Guo, G.-C. Recent Achievements on Middle and Far-Infrared Second-Order Nonlinear Optical Materials. *Coord. Chem. Rev.* **2017**, *335*, 44−57.

(3) Liu, X.; Gong, P.; Yang, Y.; Song, G.; Lin, Z. Nitrate Nonlinear Optical Crystals: A Survey on Structure-Performance Relationships. *Coord. Chem. Rev.* **2019**, *400*, No. 213045.

(4) Wang, Y.; Pan, S. Recent Development of Metal Borate Halides: Crystal Chemistry and Application in Second-Order NLO Materials. *Coord. Chem. Rev.* **2016**, *323*, 15−35.

(5) Smith, W. L. KDP and ADP Transmission in the Vacuum Ultraviolet. *Appl. Opt.* **1977**, *16*, 1798.

(6) Boyd, G. D.; Miller, R. C.; Nassau, K.; Bond, W. L.; Savage, A. $LiNbO_3$: An Efficient Phase Matchable Nonlinear Optical Material. *Appl. Phys. Lett.* **1964**, *5*, 234−236.

(7) Stolzenberger, R. A. Nonlinear Optical Properties of Flux Growth $KTiOPO_4$. *Appl. Opt.* **1988**, *27*, 3883−3886.

(8) Chen, C.; Wang, Y.; Xia, Y.; Wu, B.; Tang, D.; Wu, K.; Zeng, W.; Yu, L.; Mei, L. New Development of Nonlinear Optical Crystals for the Ultraviolet Region with Molecular Engineering Approach. *J. Appl. Phys.* **1995**, *77*, 2268−2272.

(9) Chen, C.; Wu, Y.; Jiang, A.; Wu, B.; You, G.; Li, R.; Lin, S. New Nonlinear-Optical Crystal: LiB_3O_5. *J. Opt. Soc. Am. B* **1989**, *6*, 616−621.

(10) Wu, Y.; Sasaki, T.; Nakai, S.; Yokotani, A.; Tang, H.; Chen, C. CsB_3O_5: A New Nonlinear Optical Crystal. *Appl. Phys. Lett.* **1993**, *62*, 2614−2615.

(11) Sasaki, T.; Mori, Y.; Yoshimura, M. Progress in the Growth of a $CsLiB_6O_{10}$ Crystal and Its Application to Ultraviolet Light Generation. *Opt. Mater.* **2003**, *23*, 343−351.

(12) Ohmer, M. C.; Pandey, R. Emergence of Chalcopyrites as Nonlinear Optical Materials. *MRS Bull.* **1998**, *23*, 16−22.

(13) Tarascon, J.-M.; Armand, M. Issues and Challenges Facing Rechargeable Lithium Batteries. *Nature* **2001**, *414*, 359−367.

(14) Madsen, G. K. H. Automated Search for New Thermoelectric Materials: The Case of LiZnSb. *J. Am. Chem. Soc.* **2006**, *128*, 12140−12146.

(15) Foltyn, S. R.; Civale, L.; MacManus-Driscoll, J. L.; Jia, Q. X.; Maiorov, B.; Wang, H.; Maley, M. Materials Science Challenges for High-Temperature Superconducting Wire. *Nat. Mater.* **2007**, *6*, 631−642.

(16) Gurevich, A. Challenges and Opportunities for Applications of Unconventional Superconductors. *Annu. Rev. Condens. Matter Phys.* **2014**, *5*, 35−56.

(17) Clark, S. J.; Segall, M. D.; Pickard, C. J.; Hasnip, P. J.; Probert, M. I. J.; Refson, K.; Payne, M. C. First Principles Methods Using CASTEP. *Z. Kristallogr. - Cryst. Mater.* **2005**, *220*, 567−570.

(18) Jia, W.; Fu, J.; Cao, Z.; Wang, L.; Chi, X.; Gao, W.; Wang, L.-W. Fast Plane Wave Density Functional Theory Molecular Dynamics Calculations on Multi-GPU Machines. *J. Comput. Phys.* **2013**, *251*, 102−115.

(19) Jia, W.; Cao, Z.; Wang, L.; Fu, J.; Chi, X.; Gao, W.; Wang, L.-W. The Analysis of a Plane Wave Pseudopotential Density Functional Theory Code on a GPU Machine. *Comput. Phys. Commun.* **2013**, *184*, 9−18.

(20) Nicholls, R. J.; Morris, A. J.; Pickard, C. J.; Yates, J. R. OptaDOS - A New Tool for EELS Calculations. *J. Phys.: Conf. Ser.* **2012**, *371*, No. 012062.

(21) Morris, A. J.; Nicholls, R. J.; Pickard, C. J.; Yates, J. R. OptaDOS: A Tool for Obtaining Density of States, Core-Level and

Optical Spectra from Electronic Structure Codes. *Comput. Phys. Commun.* **2014**, *185*, 1477−1485.
(22) Lin, J.; Lee, M.-H.; Liu, Z.-P.; Chen, C.; Pickard, C. J. Mechanism for Linear and Nonlinear Optical Effects in β-BaB_2O_4 Crystals. *Phys. Rev. B* **1999**, *60*, 13380−13389.
(23) Zhang, B.; Lee, M.; Yang, Z. Simulated Pressure-Induced Blue-Shift of Phase-Matching Region and Nonlinear Optical Mechanism for $K_3B_6O_{10}X$(X = Cl, Br). *Appl. Phys. Lett.* **2015**, *106*, No. 031906.
(24) Perdew, J. P.; Burke, K.; Ernzerhof, M. Generalized Gradient Approximation Made Simple. *Phys. Rev. Lett.* **1996**, *77*, 3865−3868.
(25) Read, A. J.; Needs, R. J. Calculation of Optical Matrix Elements with Nonlocal Pseudopotentials. *Phys. Rev. B* **1991**, *44*, 13071−13073.
(26) Aversa, C.; Sipe, J. E. Nonlinear Optical Susceptibilities of Semiconductors: Results with a Length-Gauge Analysis. *Phys. Rev. B* **1995**, *52*, 14636−14645.
(27) Krukau, A. V.; Vydrov, O. A.; Izmaylov, A. F.; Scuseria, G. E. Influence of the Exchange Screening Parameter on the Performance of Screened Hybrid Functionals. *J. Chem. Phys.* **2006**, *125*, No. 224106.
(28) Heyd, J.; Scuseria, G. E.; Ernzerhof, M. Hybrid Functionals Based on a Screened Coulomb Potential. *J. Chem. Phys.* **2003**, *118*, 8207−8215.
(29) Lee, M.-H.; Yang, C.-H.; Jan, J.-H. Band-Resolved Analysis of Nonlinear Optical Properties of Crystalline and Molecular Materials. *Phys. Rev. B* **2004**, *70*, No. 235110.
(30) Hu, Z.; Yue, Y.; Chen, X.; Yao, J.; Wang, J.; Lin, Z. Growth and Structure Redetermination of a Nonlinear $BaAlBO_3F_2$ Crystal. *Solid State Sci.* **2011**, *13*, 875−878.
(31) Zaitsev, A. I.; Aleksandrovskii, A. S.; Zamkov, A. V.; Sysoev, A. M. Nonlinear Optical, Piezoelectric, and Acoustic Properties of SrB_4O_7. *Inorg. Mater.* **2006**, *42*, 1360−1362.
(32) Kwon, T. Y.; Ju, J. J.; Cha, J. W.; Kim, J. N.; Yun, S. I. Characteristics of Critically Phase-Matched Second-Harmonic Generation of a $Li_2B_4O_7$ Crystal Grown by the Czochralski Method. *Mater. Lett.* **1994**, *20*, 211−215.
(33) Komatsu, R.; Sugawara, T.; Sassa, K.; Sarukura, N.; Liu, Z.; Izumida, S.; Segawa, Y.; Uda, S.; Fukuda, T.; Yamanouchi, K. Growth and Ultraviolet Application of $Li_2B_4O_7$ Crystals: Generation of the Fourth and Fifth Harmonics of Nd:$Y_3Al_5O_{12}$ Lasers. *Appl. Phys. Lett.* **1997**, *70*, 3492−3494.
(34) Sugawara, T.; Komatsu, R.; Uda, S. Growth and Characterization of Lithium Tetraborate Crystals Grown in Phase-Matching Directions. *J. Cryst. Growth* **1998**, *193*, 364−369.
(35) Fröhlich, R.; Bohatý, L.; Liebertz, J. Die Kristallstruktur von Wismutborat, BiB_3O_6. *Acta Crystallogr., Sect. C: Struct. Chem.* **1984**, *40*, 343−344.
(36) Luo, M.; Liang, F.; Song, Y.; Zhao, D.; Xu, F.; Ye, N.; Lin, Z. $M_2B_{10}O_{14}F_6$ (M = Ca, Sr): Two Noncentrosymmetric Alkaline Earth Fluorooxoborates as Promising Next-Generation Deep-Ultraviolet Nonlinear Optical Materials. *J. Am. Chem. Soc.* **2018**, *140*, 3884−3887.
(37) Zhang, Z.; Wang, Y.; Zhang, B.; Yang, Z.; Pan, S. $CaB_5O_7F_3$:A Beryllium-Free Alkaline-Earth Fluorooxoborate Exhibiting Excellent Nonlinear Optical Performances. *Inorg. Chem.* **2018**, *57*, 4820−4823.
(38) Mutailipu, M.; Zhang, M.; Zhang, B.; Wang, L.; Yang, Z.; Zhou, X.; Pan, S. $SrB_5O_7F_3$ Functionalized with $[B_5O_9F_3]^{6-}$ Chromophores: Accelerating the Rational Design of Deep-Ultraviolet Nonlinear Optical Materials. *Angew. Chem., Int. Ed.* **2018**, *57*, 6095−6099.
(39) Zhang, B.; Shi, G.; Yang, Z.; Zhang, F.; Pan, S. Fluorooxoborates: Beryllium-Free Deep-Ultraviolet Nonlinear Optical Materials without Layered Growth. *Angew. Chem., Int. Ed.* **2017**, *56*, 3916−3919.
(40) Wang, Y.; Zhang, B.; Yang, Z.; Pan, S. Cation-Tuned Synthesis of Fluorooxoborates: Towards Optimal Deep-Ultraviolet Nonlinear Optical Materials. *Angew. Chem., Int. Ed.* **2018**, *57*, 2150−2154.
(41) Shi, G.; Wang, Y.; Zhang, F.; Zhang, B.; Yang, Z.; Hou, X.; Pan, S.; Poeppelmeier, K. R. Finding the Next Deep-Ultraviolet Nonlinear Optical Material: $NH_4B_4O_6F$. *J. Am. Chem. Soc.* **2017**, *139*, 10645−10648.
(42) Logemann, C.; Wickleder, M. S. $B_2S_2O_9$: A Boron Sulfate with Phyllosilicate Topology. *Angew. Chem., Int. Ed* **2013**, *52*, 14229−14232.
(43) Ju, J.; Yang, T.; Li, G.; Liao, F.; Wang, Y.; You, L. PKU-5: An Aluminoborate with Novel Octahedral Framework Topology. *Chem. - Eur. J.* **2004**, *10*, 3901−3906.
(44) Neumair, S. C.; Sohr, G.; Vanicek, S.; Wurst, K.; Kaindl, R.; Huppertz, H. The New High-Pressure Sodium Tetraborate HP-$Na_2B_4O_7$. *Z. Anorg. Allg. Chem.* **2012**, *638*, 81−87.
(45) Marsh, R. E.; Schomaker, V. Potassium Tetraehlorosulfatoborate: Change in Space Group. *Acta Crystallogr., Sect. B: Struct. Sci., Cryst. Eng. Mater.* **1980**, *B36*, 219−220.
(46) Mairesse, G.; Drache, M. The Crystal Structure of Potassium Tetraehlorosulfatoborate, $K[B(SO_3Cl)_4]$. *Acta Crystallogr., Sect. B: Struct. Sci., Cryst. Eng. Mater.* **1978**, *B34*, 1771−1776.
(47) Shuvalov, R. R.; Burns, P. C. A New Polytype Of Orthoboric Acid, H_3BO_3-3T. *Acta Crystallogr., Sect. C: Struct. Chem.* **2003**, *C59*, i47−i49.
(48) Sun, Y. J.; Zhang, Z.; Wang, Y. L.; Yang, G. Y. Synthesis, Structure and Characterization of a New Nonlinear Optical Calcium Borate $[Ca_2B_5O_9]\cdot[H(OH)_2]$. *Inorg. Chem. Commun.* **2017**, *86*, 308−311.
(49) Wiggin, S. B.; Weller, M. T. Redetermination of $CaB_8O_{11}(OH)_4$ at Low Temperature. *Acta Crystallogr., Sect. E: Crystallogr. Commun.* **2005**, *E61*, i243−i245.
(50) Mou, X.-S.; Hu, Z.-G.; Zhang, C.-L. Hydrothermal Growth, Characterization and Nonlinear Optical Effects of $CaB_8O_{11}(OH)_4$ Crystal. *J. Synth. Cryst.* **2010**, *39*, 10−15.

https://dx.doi.org/10.1021/acs.chemmater.0c02583
Chem. Mater. 2020, 32, 6772−6779